Journal of Solid State Chemistry 233 (2016) 289–293

Contents lists available at ScienceDirect

Journal of Solid State Chemistry

journal homepage: www.elsevier.com/locate/jssc

Mechanical properties and negative thermal expansion of a dense rare earth formate framework

Zhanrui Zhang [a], Xingxing Jiang [b], Guoqiang Feng [c], Zheshuai Lin [b], Bing Hu [d,*], Wei Li [c,*]

[a] School of Materials Science and Engineering, Huazhong University of Science and Technology, Wuhan 430074, China
[b] Center for Crystal R&D, Key Lab of Functional Crystals and Laser Technology of Chinese Academy of Sciences, Technical Institute of Physics and Chemistry, Chinese Academy of Sciences, Beijing 100190, China
[c] School of Physics and Wuhan National High Magnetic Field Center, Huazhong University of Science and Technology, Wuhan 430074, China
[d] Fujian Institute of Research on the Structure of Matter, Chinese Academy of Sciences, Fuzhou 350002, China

ARTICLE INFO

Article history:
Received 23 September 2015
Received in revised form
23 October 2015
Accepted 30 October 2015
Available online 31 October 2015

Keywords:
Metal–organic frameworks
Mechanical properties
Nanoindentation
Thermal expansion

ABSTRACT

The fundamental mechanical properties of a dense metal–organic framework material, $[NH_2CHNH_2][Er(HCOO)_4]$ (**1**), have been studied using nanoindentation technique. The results demonstrate that the elastic moduli, hardnesses, and yield stresses on the (021)/(02 − 1) facets are 29.8/30.2, 1.80/1.83 and 0.93/1.01 GPa, respectively. Moreover, variable-temperature powder and single-crystal X-ray diffraction experiments reveal that framework **1** shows significant negative thermal expansion along its *b* axis, which can be explained by using a hinge–strut structural motif.

1. Introduction

Metal–organic frameworks (MOFs) are a young class of crystalline materials in which inorganic and organic entities are integrated homogeneously *via* coordination bonding. According to their structural nature, they can be categorized into two subclasses: porous and dense phases. Numerous porous MOFs have been designed and created in the last decade [1], apparently because they have shown great potential for applications beyond traditional porous materials (*i.e.* porous carbon and zeolites) [2,3]. In addition to many studies on porous MOFs [4–6], research interests in the field of dense phases have also been growing significantly since they can show many fascinating physical properties which are traditionally dominated by inorganics [1–3].

Despite a great number of studies on the properties of MOFs, research about their mechanical properties, which are critical to many aspects of the industrial manufacturing and processing, should be strengthened, particularly in light of the imminence of the aforementioned applications [7–10]. Cheetham group and other researchers have systematically explored the basic mechanical properties and structure–property relationships of several series of dense MOFs constructed from first row transitional metals, yet there are only few studies about dense rare earth MOFs [11,12]. Herein, we use nanoindentation technique to study the fundamental elastic and plastic properties of a rare earth formate framework, $[NH_2CHNH_2][Er(HCOO)_4]$ (**1**). In addition, variable-temperature single-crystal and powder X-ray diffraction experiments reveal that **1** exhibits negative thermal expansion (NTE) behavior along its *b*-axis.

2. Experimental section

2.1. Synthesis

All chemicals and solvents were of reagent grade and used as received. The title framework was prepared using a previously published method [13].

2.2. Nanoindentation experiment

Nanoindentation was performed at ambient temperature using an MTS NanoIndenter® XP (MTS Corp., Eden Prairie, MN). Untwinned single crystals were face-indexed *via* single crystal X-ray diffraction. The (021) or (02 − 1) facets of samples were selected as testing surface [14]. The strain rates of loading and unloading procedure were set at $5 \times 10^{-2}\ s^{-1}$. To minimize creep effects, at the maximum displacement of 1000 nm which is the point prior to unloading, the indenter was held for 30 s. For calibration, a fused silica standard with an elastic modulus of 72 GPa and hardness of 9 GPa was employed.

* Corresponding author.
E-mail addresses: hubing@fjirsm.ac.cn (B. Hu), wl276@hust.edu.cn (W. Li).

http://dx.doi.org/10.1016/j.jssc.2015.10.043
0022-4596/

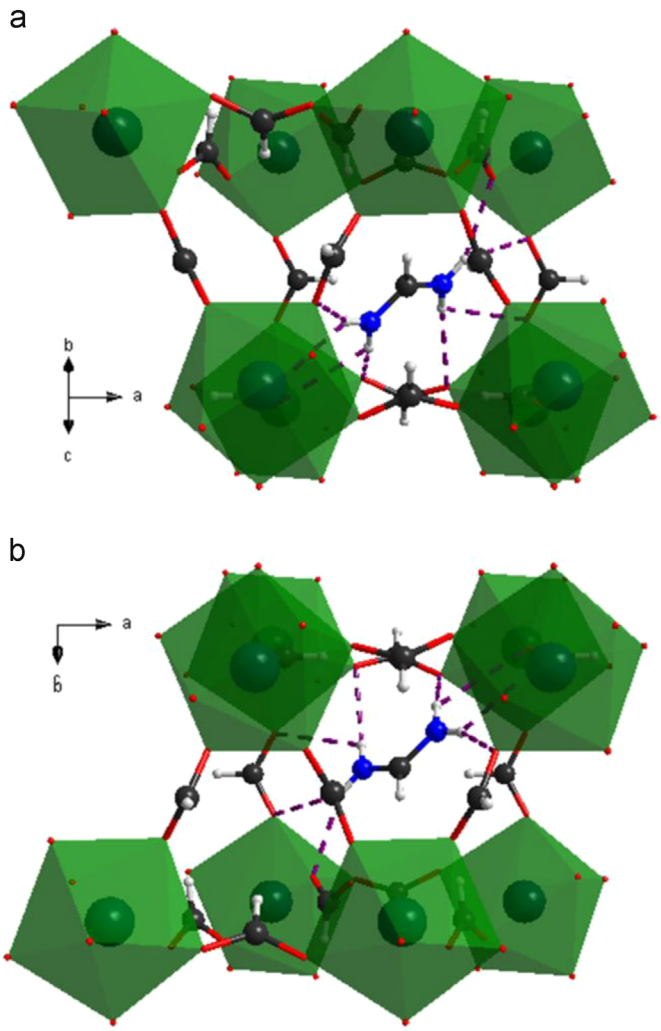

Fig. 1. Crystal structure of framework 1 viewed along the (021) (a) and (02 – 1) direction (b).

2.2.1. *Young's modulus and hardness*

To determine the Young's modulus (E) and hardness (H), a three sided pyramidal Berkovich indenter with a sharp tip (end radius ~100 nm) was used. The elastic modulus of the diamond indenter is 1141 GPa and the Poisson's ratio is 0.07. The elastic moduli of the sample were calculated with an assumptive Poisson's ratio of 0.3. Young's modulus (E_s) and indentation hardness (H) of the framework **1** were obtained from the P–h curves using the standard Oliver–Pharr Method [15,16].

2.2.2. *Elastic–plastic transition*

For the investigation of elastic–plastic transition, a spherical tip indenter (radius ~10 μm) was used. According to published procedures, the indentation stress and strain were obtained from the relationship:

$$P_m = \frac{4E_r}{3\pi}\left(\frac{a}{R}\right)$$

P_m represents the indentation stress, a is the contact radius and R represents the radius of the spherical tip. The strain was determined by a/R [17,18].

2.3. *Variable-temperature single crystal X-ray diffraction*

Single-crystal X-ray diffraction was performed on an Oxford Diffraction Gemini E Ultra diffractometer using Mo radiation

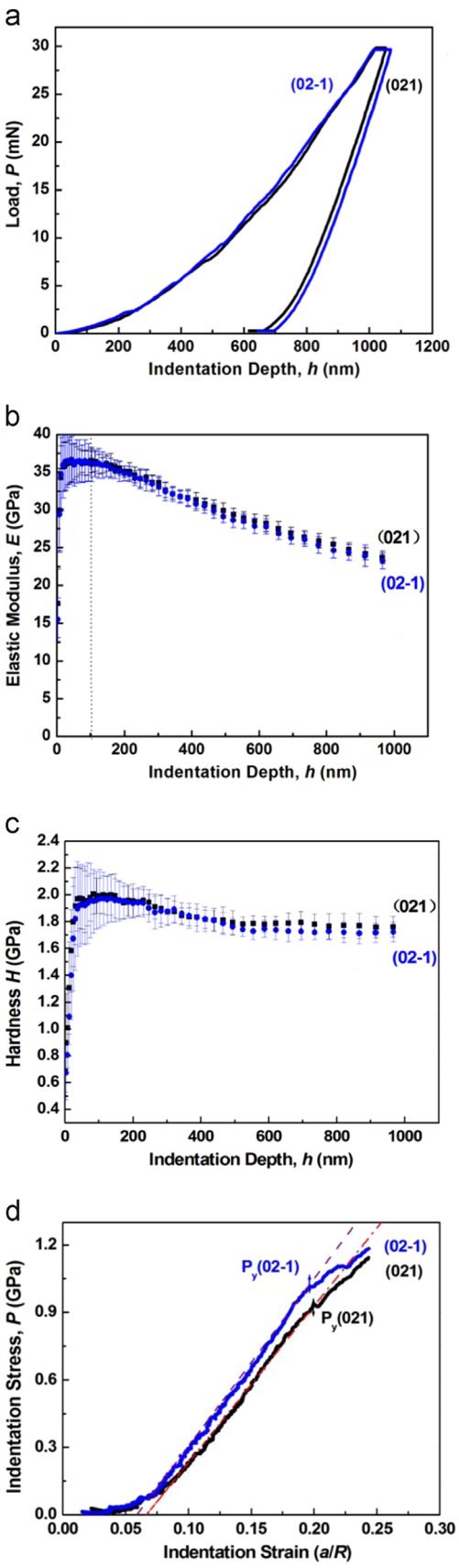

Fig. 2. Data of nanoindentation experiments obtained normal to (021) and (02 – 1) planes of single crystal framework **1** (a) load–displacement (P–h) curves; (b) Elastic moduli as a function of indentation depth; (c) Hardnesses as a function of indentation depth; (d) Indentation stresses as a function of indentation strain. Dotted lines represent the linear Hookean fits of experimental data.

Table 1
Mechanical properties of related frameworks reported in the previous research.

Dense MOFs	E (GPa)	H (GPa)	D_c (g cm^{-1})	P_y (GPa)	References
$Cu_3(H_2O)_2[O_3PCH_2CO_2]_2$ (polymorph I)	50–93	4.2–4.7	2.934	1.8–2.3	[14]
$Cu_3(H_2O)_2[O_3PCH_2CO_2]_2$ (polymorph II)	35–61	2.3–2.5	2.954	0.7–1.9	[14]
$Ce(C_2O_4)(HCO_2)$	43–78	3.9–4.6	3.395	1.2–2.0	[23]
[AmineH$^+$][M(HCO$_2$)$_3$][a]	12–29	0.8–1.0	1.71–1.85	–	[24,25]
Framework **1**	30	1.8	2.530	0.9–1.0	
Porous MOFs	E (GPa)	H (GPa)	D_c (g cm^{-1})	P_y	References
ZIFs	3–9	0.2–1.1	0.95–1.56	–	[19–21]
[Zn2(L)$_2$(dabco)][b]	2–10	0.2–0.5	0.95–1.31	–	[22]

[a] AmineH$^+$ = methylammonium, gunidinium and azetidinium; M = Mn and Zn.
[b] L = 1,4-benzenedicarboxylate derivative and dabco = 1,4-diazabicyclo[2.2.2]octane.

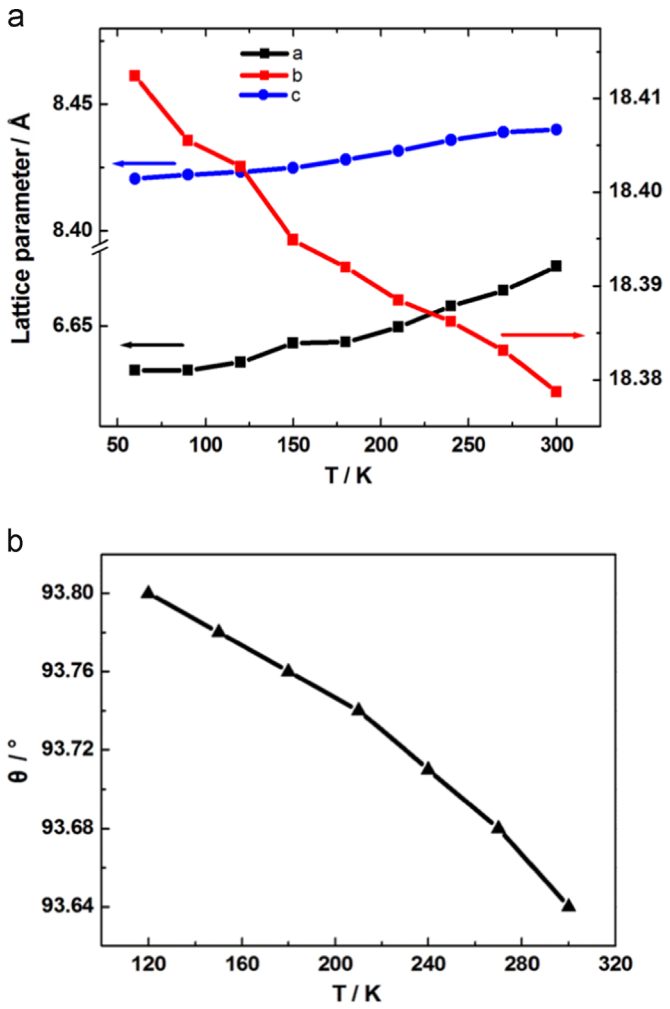

Fig. 3. (a) Evolution of lattice parameters a, b and c in dependence on the temperature (the solid lines are there to guide the eye); (b) The change of hinge angle θ as a function of temperature.

(λ = 0.71073 Å). Full data sets of framework **1** were collected from 120 to 300 K at intervals of 30 K. Data collection, cell determination and refinement and data reduction were performed using *CrysAlisPro* software. All the structures were solved using direct methods and successive Fourier difference syntheses, and refined by full matrix least-squares procedure on F^2 with anisotropic thermal parameters for all non-hydrogen atoms, using the SHELXTL-97[6] package of programs *via* the X-Seed interface. All hydrogen atoms were located by geometric calculations and refined using a riding mode and isotropic displacement parameters constrained to 1.2 times those of their adjacent carbon or nitrogen atoms. CCDC-1412167 to 1412173 contain the Supplementary crystallographic data for this paper. These data can be obtained free of charge from The Cambridge Crystallographic Data Centre *via* www.ccdc.cam.ac.uk/data_request/cif.

2.4. Variable-temperature powder X-ray diffraction

The *in-situ* low-temperature X-ray powder diffraction patterns were collected on a Bruker D8-discover X-ray diffractometer. The detailed equipment parameters were: Cu $K\alpha$ radiation ($K\alpha_1$ = 1.5406 Å and $K\alpha_2$ = 1.5443 Å), 40 kV; 30 mA; 2 mm divergence slit; 0.6 mm anti-scatter slit; 0.2 mm receiving slit; monochromatic; 0.1 mm detector slit. The temperature was controlled by a cryostat with the temperature-controlling error less than 1 K. To guarantee the sufficient relaxation of the cell parameters with the decreasing temperature, the temperature-decreasing rate and soaking time at every temperature were set to 10 K/s and 5 min respectively. The angular scanning range was 10–50° with the step of 0.01° and scanning rate 1 s/step. The cell parameters of the variable temperatures were refined by the Rietveld method using GSAS software.

3. Results and discussion

3.1. Crystal structure description

Framework **1** has a chiral structure and crystalizes in $C222_1$ space group at ambient conditions. In the structure, the Er^{3+} ion is coordinated by eight *anti–anti* $HCOO^-$ ligands to form an ErO_8 polyhedron, and each ErO_8 is linked to six neighboring polyhedra to constitute a NaCl-like $[Er(HCOO)_4]^-$ framework structure with $NH_2CHNH_2^+$ cation located in the framework cavities (Fig. 1) [13]. Apart from six orthogonal formate linkages along three principle axes, there are two additional diagonal ones lying in the *bc* plane.

3.2. Mechanical properties

Nanoindentation experiments reveal the characteristic mechanical properties of framework **1**. Representative load–penetration (P–h) curves obtained on all facets of framework are shown in Fig. 2(a). And as shown in Fig. 2(b), the E of the (021) and (02 − 1) facets are 30.2 (5) and 29.8(8) GPa, and the H are 1.83(5) and 1.80(6) GPa, respectively. Though there is no inversion center between the (021) and (02 − 1) planes due to the chiral 2_1 axis in framework **1**, the structural difference between them is very subtle (Fig. 1). Therefore, these two facets exhibit identical stiffness and hardness as observed from the above nanoindentation data. Indentation on other factes of **1** can not be realized due to the crystal morphology, which hinders better

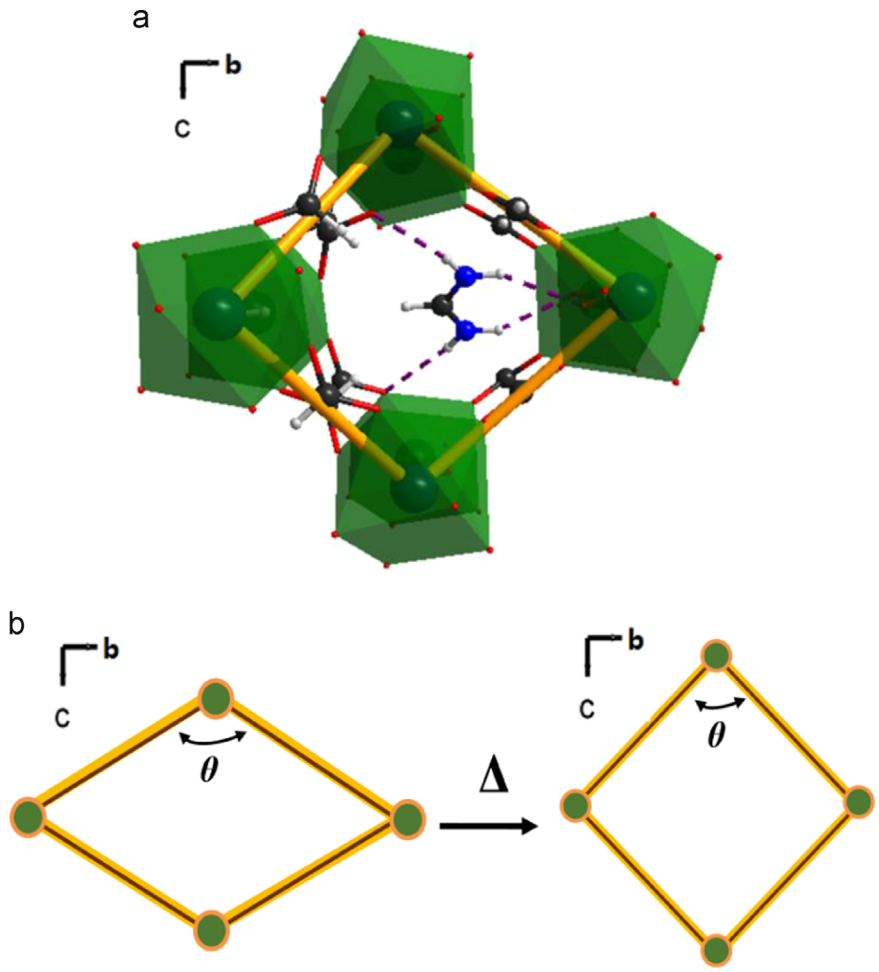

Fig. 4. Thermal expansion mechanism of framework **1**. (a) The yellow frames represent hinge–strut like structure; (b) The decreasing of θ, from 93.80° at 120 K to 93.64° at 300 K, results in NTE along the *b* axis. (For interpretation of the references to color in this figure legend, the reader is referred to the web version of this article.)

Table 2
Hydrogen bonds lengths (Å) and bond angles (deg) of framework 1 at 120 and 300 K.

D–H···A	Lengths (Å) @120 K	@300 K	Angle (deg) @120 K	@300 K
$N(1)^a$–$H(1B)^a$···$O(3)^c$	2.9733(8)	2.9881(9)	153.387(5)	153.457(5)
$N(1)^a$–$H(1B)^a$···$O(2)^d$	3.0540(9)	3.0759(1)	130.102(4)	130.981(6)
$N(1)^a$–$H(1A)^a$···$O(2)^a$	3.1921(9)	3.2196(1)	118.976(4)	118.613(5)
$N(1)^a$–$H(1A)^a$···$O(1)^a$	3.0213(8)	3.0287(9)	153.866(5)	154.946(5)
$N(1)^b$–$H(1A)^b$···$O(1)^b$	3.0213(8)	3.0287(9)	153.866(5)	154.946(5)
$N(1)^b$–$H(1A)^b$···$O(2)^b$	3.1921(9)	3.2196(1)	118.976(4)	118.613(5)
$N(1)^b$–$H(1B)^b$···$O(2)^e$	3.0540(9)	3.0759(1)	130.102(4)	130.981(6)
$N(1)^b$–$H(1B)^b$···$O(3)^f$	2.9733(8)	2.9881(9)	153.387(5)	153.457(5)

Symmetry code: (*a*) $-0.5-x$, $-0.5+y$, $0.5-z$; (*b*) $0.5+x$, $-0.5+y$, z; (*c*) $-0.5+x$, $-0.5-y$, $-z$; (*d*) $-0.5-x$, $-0.5-y$, $-0.5+z$; (*e*) $0.5+x$, $-0.5-y$, $1-z$; (*f*) $0.5-x$, $-0.5-y$, $0.5+z$.

mapping of elastic and plastic properties of **1**. As listed in Table 1, the average *E* and *H* values of framework **1** are an order of magnitude higher than those from porous ZIFs [19–21] and $[Zn_2(L)_2(dabco)]$ [22], which can be attributed to the dense packing nature of structure in **1**. Compared with those of $Cu_3(H_2O)_2[O_3PCH_2CO_2]_2$ [14] and $Ce(C_2O_4)(HCO_2)$ [23], the *E* and *H* values of **1** are significantly lower due to its less dense structure as well as the existence of more rigid Cu–O–Cu chains and oxalate ligands in the former. Additional comparison with dense metal–formate frameworks with perovskite architecture, $[AmineH^+][M^{II}(HCOO)_3]$ [24,25], show that the *E* and *H* values of **1** are much higher than those less hydrogen bonded $[(CH_3)_2NH_2^+][M^{II}(HCOO)^3]$ (M=Mn, Co, Ni and Zn) [24] and $[(CH_2)_3NH^+][Mn(HCOO)_3]$ [25], but comparable with strongly hydrogen bonded $[(NH_2)_3C][Mn(HCOO)_3]$ [25]. These differences can be explained by considering the existence of bridging and strong hydrogen bonding mode in **1**.

In addition, the elastic–plastic transition behavior of the two facets were studied *via* indentation using a spherical tip. The yield stress, P_y, represents the transitional stress from elastic to plastic deformation (point of deviation from Hookean linearity). As shown in Fig. 2(d), the $P_{y(021)}$ and $P_{y(02-1)}$ are 0.93(6) and 1.01(3) GPa, respectively, which are lower than those from the denser $Cu_3(H_2O)_2[O_3PCH_2CO_2]_2$ and $Ce(C_2O_4)(HCO_2)$ [14,23–27]. The above significant differences between **1** and $Cu_3(H_2O)_2[O_3PCH_2CO_2]_2$ or $Ce(C_2O_4)(HCO_2)$ can be explained by the presence of oxide chains and oxalate ligands in these MOFs, which are more rigid than the formate linker.

3.3. Thermal expansion study

Thermal expansion behaviour of framework **1** was studied *via* variable-temperature powder X-ray diffraction (VT–PXRD) experiments. The measured temperature-dependent variations in the lattice parameters between 60 and 300 K with a 30 K interval are shown in Fig. 3(a). Axes *a* and *c* show positive thermal expansion (PTE) about +0.33% and +0.25%, respectively, whereas *b* axis exhibits negative thermal expansion (NTE) about −0.18%. The average coefficients of thermal expansion along three orthogonal axes and the volumetric thermal expansion coefficient are

$\alpha_a = 11.7(11)$, $\alpha_b = -7.1(3)$, $\alpha_c = 10.0(7)$ and $\alpha_V = 16.5(15)\ MK^{-1}$, respectively, obtained *via* linear fits using the PASCal software [28]. It is noteworthy that the NTE of *b* axis is about the same magnitude of that from the most well-known NTE material cubic zirconium tungstate, ZrW_2O_8 (for which $\alpha = -9\ MK^{-1}$) [29]. Compared with some prototypical NTE MOFs [30–34], the NTE magnitude of **1** is slightly smaller than that from rigid MOF-5 ($\alpha = -9\ MK^{-1}$) [32], but significantly lower than those from flexible silver(I) 2-methylimidazolate ($\alpha_c = -24.5\ MK^{-1}$) [30], $[Zn_2(fu\text{-}L)_2dabco]$ (fu-L=alkoxy functionalized 1,4-benzenedicarboxylate, dabco=1,4-diazabicyclo [2.2.2]octane; $\alpha_x = -94.3$ to $-129\ MK^{-1}$) [31], CdI_2[meso-tetra(4-pyridyl)porphine] ($\alpha_b = -21\ MK^{-1}$) [33] and $In(BDC)_2$ (BDC=1,4-benzenedicarboxylate; $\alpha_c = -35\ MK^{-1}$) [34].

To elucidate the NTE mechanism of framework **1**, we collected variable-temperature single crystal X-ray diffraction (VT-SCXRD) data from 120 to 300 K with a 30 K interval. The data at all temperature points were solved and compared to give insights about the underlying structural origin. As shown in Fig. 4, framework **1** can be considered as a hinge–strut like structure which is a prototypical motif for anisotropic thermal expansion (the formate ligand and Er(III) stand for the hinge and strut, respectively; the hinge angle is represented as θ) [30,33]. The hydrogen bond lengths in framework **1** increase slightly with ascending temperature, which induces the twist of formate ligands and the deformation of the rhombohedral unit. Specifically, all N···O bond lengths and N–H···O bond angles increase with increasing temperature apart from $N(1)^a$–$H(1A)^a$···$O(2)^a$ and $N(1)^b$–$H(1A)^b$···$O(2)^b$, as presented in Table 2. These distorsions result in the decrease of the hinge angle θ with increasing temperature, from 93.80° at 120 K to 93.64° at 300 K. The change of the hinge angle gives rise to the NTE along the *b* axis but PTE along the *a* and *c* axes. Similar mechanism has been used to explain the anisotropic thermal expansion of many hinged [30,31] and lattice fence MOFs [33]. Although framework **1** exhibits a hinged structure, the hydrogen bonding between the host $[Er(HCOO)_4]^-$ and guest ammonium is quite strong and constrains the framework to move freely to some extent. Such hinge motion in **1** is considerably less compared with those from other porous MOFs in which the host–guest interactions are dominated by weaker Van der Waals force, *i.e.* $[Zn_2(fu\text{-}L)_2dabco]$. Therefore, the corresponding higher degree of strains in framework **1** results in an order of magnitude lower NTE behaviour.

4. Conclusions

In summary, the Young's modulus, hardness and elastic–plastic transition properties of $[NH_2CHNH_2][Er(HCOO)_4]$ have been studied, which show representative characteristics like other dense MOFs. Further VT–PXRD measurements show that this MOF exhibits considerable NTE behaviour along its *b* axis. Detailed structural analysis from VT-SCXRD reveals that the anomalous thermal expansion phenomena are attributed to a hinge–strut framework motif.

Acknowledgments

Z.Z., G.F. and W.L. acknowledge funding support from the Opening Project of the Key Laboratory of Cryogenics in the Technical Institute of Physics and Chemistry, Chinese Academy of Sciences, and National Natural Science Foundation of China (Grant no. 61138006 and 21571072).

Appendix A. Supplementary material

Supplementary data associated with this article can be found in the online version at http://dx.doi.org/10.1016/j.jssc.2015.10.043.

References

[1] A.K. Cheetham, C.N.R. Rao, R.K. Feller, Chem. Commun. 46 (2006) 4780–4795.
[2] P. Horcajada, R. Gref, T. Baati, P.K. Allan, G. Maurin, P. Couvreur, G. Férey, R. E. Morris, C. Serre, Chem. Rev. 112 (2012) 1232–1268.
[3] J.-R. Li, R.J. Kuppler, H.-C. Zhou, Chem. Soc. Rev. 40 (2009) 1477–1504.
[4] H. Furukawa, K.E. Cordova, M. O'Keeffe, O.M. Yaghi, Science 341 (2013) 1230444.
[5] S. Kitagawa, R. Kitaura, S.I. Noro, Angew. Chem. Int. Ed. 43 (2004) 2334–2375.
[6] S.T. Meek, J.A. Greathouse, M.D. Allendorf, Adv. Mater. 23 (2011) 249–267.
[7] C.N.R. Rao, A.K. Cheetham, A. Thirumurugan, J. Phys. Condens. Matter 20 (2008) 2905–2910.
[8] A.K. Cheetham, C.N.R. Rao, Science 318 (2007) 58–59.
[9] P. Jain, N.S. Dalal, B.H. Toby, H.W. Kroto, A.K. Cheetham, J. Am. Chem. Soc. 130 (2008) 10450–10451.
[10] D. Bahr, J. Reid, W. Mook, C. Bauer, R. Stumpf, A. Skulan, N. Moody, B. Simmons, M. Shindel, M. Allendorf, Phys. Rev. B 76 (2007) 184106.
[11] J.C. Tan, A.K. Cheetham, Chem. Soc. Rev. 40 (2011) 1059–1080.
[12] W. Li, S. Henke, A.K. Cheetham, APL Mater. 2 (2014) 123902.
[13] B. Liu, H.B. Zheng, Z.M. Wang, S. Gao, CrystEngComm 13 (2011) 5285–5288.
[14] J.C. Tan, C.A. Merrill, J.B. Orton, A.K. Cheetham, Acta Mater. 57 (2009) 3481–3496.
[15] W.C. Oliver, G.M. Pharr, J. Mater. Res. 7 (1992) 1564–1583.
[16] W.C. Oliver, G.M. Pharr, J. Mater. Res. 19 (2004) 3–20.
[17] I.J. Spary, A.J. Bushby, N.M. Jennett, Philos. Mag. 86 (2006) 5581–5593.
[18] J.S. Field, M.V. Swain, J. Mater. Res. 8 (1993) 297–306.
[19] T.D. Bennett, J.C. Tan, S.A. Moggach, R. Galvelis, M.D. Caroline, B.A. Reisner, A. Thirumurugan, D.R. Allan, A.K. Cheetham, Chem. Eur. J. 16 (2010) 10684–10690.
[20] J.C. Tan, T.D. Bennett, A.K. Cheetham, Proc. Natl. Acad. Sci. USA 107 (2010) 9938–9943.
[21] J.C. Tan, B. Civalleri, C.C. Lin, L. Valenzano, R. Galvelis, P.F. Chen, T.D. Bennett, C. Mellot-Draznieks, C.M. Zicovich-Wilson, A.K. Cheetham, Phys. Rev. Lett. 108 (2012) 095502.
[22] S. Henke, W. Li, A.K. Cheetham, Chem. Sci. 5 (2014) 2392–2397.
[23] J.C. Tan, J.D. Furman, A.K. Cheetham, J. Am. Chem. Soc. 131 (2009) 14252–14254.
[24] J.-C. Tan, P. Jain, A.K. Cheetham, Dalton Trans. 41 (2012) 3949–3952.
[25] W. Li, A. Thirumurugan, P.T. Barton, Z. Lin, S. Henke, H.H. Yeung, M. Wharmby, E.G. Bithell, C.J. Howard, A.K. Cheetham, J. Am. Chem. Soc. 136 (2014) 7801–7804.
[26] S. Varughese, M.S.R.N. Kiran, U. Ramamurty, G.R. Desiraju, Angew. Chem. Int. Ed. 52 (2013) 2701–2712.
[27] U. Ramamurty, J.I. Jang, CrystEngComm 16 (2013) 12–23.
[28] M.J. Cliffe, A.L. Goodwin, J. Appl. Cryst. 45 (2012) 1321–1329.
[29] A. Mary, J.S.O. Evans, T. Vogt, A.W. Sleight, Science 272 (1996) 90–92.
[30] J.M. Ogborn, I. Collings, S.A. Moggach, A.L. Thompson, A.L. Goodwin, Chem. Sci. 3 (2012) 3011–3017.
[31] S. Henke, A. Schneemann, R.A. Fischer, Adv. Funct. Mater. 23 (2013) 5990–5996.
[32] N. Lock, Y. Wu, M. Christensen, L.J. Cameron, V.K. Peterson, A.J. Bridgeman, C. J. Kepert, B.B. Iversen, J. Phys. Chem. C 114 (2010) 16181–16186.
[33] L.D. DeVries, P.M. Barron, E.P. Hurley, C. Hu, W. Choe, J. Am. Chem. Soc. 133 (2011) 14848–14851.
[34] I.E. Collings, M.G. Tucker, D.A. Keen, A.L. Goodwin, CrystEngComm 16 (2014) 3498–3506.